Physica Scripta

PAPER

Nonlinear particle trapping by coherent waves in thermal and nonthermal plasmas

IOP Publishing Phys. Scr. 96 (2021) 105604 https://doi.org/10.1088/1402-4896/ac1027

Physica Scripta

RECEIVED
26 February 2021

REVISED
23 June 2021

ACCEPTED FOR PUBLICATION
30 June 2021

PUBLISHED
12 July 2021

PAPER

Nonlinear particle trapping by coherent waves in thermal and nonthermal plasmas

Pankaj K Soni , Harikrishnan Aravindakshan , Bharati Kakad and Amar Kakad

Indian Institute of Geomagnetism, New Panvel, Navi Mumbai, 410218, India

E-mail: pankajs123321@gmail.com

Keywords: plasma waves, nonlinear waves, test particle simulation, nonthermal distribution

Abstract

We perform a test particle simulation to study the resonant interaction of electrons with a stationary electrostatic wave. In the simulation, we use a new method to generate nonthermal particle distributions efficiently. This method utilizes inverse cumulative distribution function, and compared with the existing methods in the literature, found to have a negligible deviation from the analytical form of the distribution, particularly in the tail side, where nonthermal particles are situated. The simulation revealed that the trapped particle density varies highly with the width (≈10%–60%) and amplitude (≈13%–19%) of the wave potential. The particle trapping is found to be more efficient in nonthermal plasmas than thermal plasma. It implies that particle transport through waves could be more effective in nonthermal plasmas than thermal plasmas. In addition, the simulation sheds light on the particle trapping time and its relation to the characteristics of the wave potential. Overall, the present study will be helpful to understand the particle trapping by the coherent waves, which are frequently seen in space and astrophysical plasmas.

1. Introduction

Wave-particle interactions is a topic of fundamental interest in various laboratory [1, 2] and space [3] plasma-based applications, including (but not limited to) beat wave acceleration [4], formation of the magnetopause boundary [5], precipitation of particles causing auroras [6], generation of electromagnetic outer zone chorus and plasmaspheric hiss emission [7], to mention a few. Interaction of charged particles having a particular background distribution (thermal or nonthermal) with the electric or magnetic fields associated with waves controls their dynamic variability [8, 9]. This wave-particle interaction happens only when the frequency of a wave is comparable to a characteristic frequency of one or more of the three periodic motions (i.e. gyro, bounce, and drift) [10, 11]. Such nonlinear wave-particle interactions are responsible for the many space and astrophysical plasma effects, like particle acceleration/deceleration, trapping, particle scattering, etc [12]. The particles having velocities less (greater) than the wave phase velocity are accelerated (decelerated) by the wave field to move with the wave phase velocity [13]. When the potential associated with the wave is larger than the thermal energy of particles, i.e. $\phi > \frac{k_B T}{e}$, the particles will get trapped inside the wave potential and confined to a finite zone of phase space, where they rebound back and forth [14, 15]. When an energetic particle propagates in a collisionless system with counter-propagating waves, it can simultaneously scatter off waves propagating in both directions [16].

Several studies have been carried out to investigate the nonlinear resonance interactions between wave and particles. Bernstein, Greene, and Kruskal (BGK) [17] have introduced the concept of nonlinear particle trapping by investigating a one-dimensional stationary nonlinear electrostatic wave in electron-ion plasma system. Krasovsky *et al* [18] had derived the condition for particle trapping in the symmetric potential with a uniform background magnetic field by considering the finite gyroradius effect within the framework of the adiabatic theory. Artemyev *et al* [19] used a theoretical model to investigate the evolution of the charged particle distribution function in a system with nonlinear wave-particle interactions and demonstrated that particle motion could be characterized by the probability of tapping into the wave's resonance. However, a crucial issue is to examine the characteristics of short-term interactions of the individual particle with a wave-potential along with the full-time evolution of the particle distribution function. The rapid change in phase space due to wave-particle interaction via trapping is challenging to examine by theoretical models.

Besides, as the trapped particle density is a function of velocity, the plasma's distribution function also plays a vital role in space plasma dynamics [20–23]. Mechanisms such as particle acceleration, plasma heating, wave-particle interaction, etc may lead to electron distributions with an increased relative weight of the nonthermal component of the distribution function, where a power-law dependence may be observed [24]. The spacecraft observations unveiled that kappa (κ) distribution represents a more realistic picture, and the assumption of space plasma being in the state of thermal equilibrium is absurd. The index κ (the distribution function spectral index), for which the kappa distribution is called, is the strength of distribution [25]. Various studies have provided theoretical backing to develop plasma theories and simulations based on kappa distribution [26–29]. Thus, a study of nonlinear trapping of particles by waves sensitive to plasma distribution is imperative.

To understand the trapping mechanism and its dependence on a particle distribution function, the generation of particles following particular distribution functions is pivotal. There are standard techniques (like, normal random deviates) to generate particles following the Maxwellian distribution function. However, the generation of an ensemble of particles that follow nonthermal (kappa) distribution is tricky. There are attempts to incorporate the kappa distribution into the simulation model. Robert *et al* [30] used the accept-reject method to generate particles that follow kappa distribution. In this method, initially, particles are distributed uniformly in the velocity space and then accepted only those particles that fall in the distribution. Therefore, one has to establish bounds for the target analytically deviates' ratio, which makes this method computationally expensive [31]. On the other hand, Abdul and Mace [32] distributed pseudo-random deviates following the kappa distribution using generalized student t-distribution. Generating kappa distributed particles using student t-distribution is around 20 times faster than the accept-reject method [32]. However, this method shows undesirable deviation, especially in the tail side of the distribution, where the higher energy particles are situated. Thus, a new method to generate particle distributions with more accuracy in the simulation is crucial.

In this context, first, we have presented a new approach for generating the particles following the kappa distribution using the inverse cumulative distribution function (CDF) method. The method is then compared with the exiting student t-distribution method and the theoretical expression, and their deviations are calculated. Next, the test-particle simulation approach is used to analyze the nonlinear wave-particle interaction by examining the behavior of an individual particle along with the information of temporal change in the particle distribution function. Although there were theoretical attempts to study the characteristics of waves probing the role of background plasma distribution function and morphology of wave-potential, a simulation study is yet to realize. For this, test particle simulation is a reasonable approach to examine the particle trapping mechanism along with its dependence on a particle distribution function and wave-potential properties [33, 34].

We conduct a series of test-particle simulations to investigate the role of particle distribution function (thermal or nonthermal) of ambient plasma on the trapping characteristics in the presence of a stationary coherent wave-potential with a Gaussian form. We have investigated the variation of particle trapping density with the amplitude and width of wave-potential. Furthermore, we have initiated the particles following a particular distribution in the presence of wave-potential and examined the time evolution of particle distribution function. Subsequently, we performed simulations to examine the change in the trapping density and time with the wave potential's distribution functions, amplitude, and width. The paper is organized as follows. The simulation model and theoretical formalism are presented in section 2. The results are discussed in section 3. Finally, the results are concluded in section 4.

2. Simulation model

In the simulation system, we need a wave potential and electrons following either thermal or nonthermal distribution functions to understand their role in particle trapping. We consider a test particle simulation by taking a large number of electrons. For this purpose, initially, we have to distribute the ambient plasma particles following thermal (Maxwellian) or nonthermal (kappa) distribution function. The method adopted to distribute particles in nonthermal and thermal distribution is described in the following subsection.

2.1. Generating nonthermal particle distribution function

The observations suggest that the plasma is often not in the thermal equilibrium in the near-Earth and astrophysical plasma environments. Such nonthermal plasma can be described with kappa (κ) distribution function [22, 28, 35, 36], and the references therin. In such a scenario, it is required to incorporate the kappa distribution function apart from the usual thermal distribution to describe the simulation model's ambient plasma. There are standard methods to incorporate thermal distribution function in simulation model [37, 38]. For example, one can generate it from the set of random normal deviates, and it is the standard method adopted in several simulations. Similarly, there were some attempts to incorporate the kappa distribution into the simulation model for nonthermal distribution functions. For example, Robert *et al* [30] used the accept-reject method to generate a flock of particles that follow kappa distribution. Abdul *et al* [32] distributed pseudo-random deviates following the kappa distribution by using the generalized student t-distribution. An important limitation of the accept-reject method is that one has to establish bounds for the target and proposal densities ratio analytically. There is a lack of general procedures for the computation of tight bounds [31]. The accept-reject method initially generates particles uniformly in the velocity space and accepts only those particles that fall in the distribution. Therefore, this method is computationally expensive [32]. On the other hand, generating kappa distributed particles using student t-distribution is around 20 times faster than the accept-reject method [32]. However, the kappa distribution generated using student t-distribution shows undesirable deviation, especially in the tail side, where the higher energy particles are situated. To overcome this problem, we present a new method, which is accurate and computationally reasonable to generate the particles following kappa distribution for general purposes. The conventional one-dimensional kappa distribution is given by following equation [26, 29],

$$f(v) = \frac{n_0}{\sqrt{\pi}v_{th}}\frac{1}{\kappa(2\kappa-3)^{1/2}}\frac{\Gamma(\kappa+1)}{\Gamma\left(\kappa-\frac{1}{2}\right)}\left(1+\frac{v^2}{(2\kappa-3)v_{th}^2}\right)^{-\kappa} \tag{1}$$

Here, Γ is Gamma function, $v_{th} = (k_B T/m)^{1/2}$ is thermal velocity of particles. The spectral index, κ is a measure of the slope of the energy spectrum of particles that decides the shape of the kappa distribution's tail. κ-index should always be greater than 1.5. A smaller value of κ means the shallower slope, and it represents the long tail velocity distribution function to ensure the presence of high-energy particles. As κ tends to ∞, the distribution function tends to attain the thermal distribution. Here, we used the inverse CDF to generate particles in the velocity space following the kappa distribution. This technique uses the fact that for a continuous CDF, the function $f(v)$ is a one-to-one mapping of the domain of CDF for a fixed interval between (0, v). The CDF of kappa distribution can be obtained by integrating equation (1) in an interval of 0 to v. The analytical expression of the CDF of kappa distribution is given by,

$$F(v) = \int_0^v f(v)dv = \frac{n_0}{\sqrt{\pi}v_{th}}\frac{v}{\kappa(2\kappa-3)^{1/2}}\frac{\Gamma(\kappa+1)}{\Gamma(\kappa-0.5)} \times {}_2F_1\left[0.5,\ \kappa,\ 1.5,\ \frac{-v^2}{v_{th}^2(2\kappa-3)}\right] \tag{2}$$

Here, n_0 is the particle density (number of particles per unit Debye length), and v_{th} is thermal speed. The inverse CDF can be used for one to one mapping to generate the particles following kappa distribution. For this, the required input parameters are: kappa index (κ), number of particles (n), thermal and drift velocities (v_{th}, and v_d). In this method, first, we are generating a very high number of particles (like, $N_p = 2^{24}$), and than choosing n particles from them using bit-reversed number generator to get sufficient nonthermal particles. Moreover, It may be noted that the CDF, $F(v)$ of kappa distribution includes the Gauss hypergeometric function ${}_2F_1$. The computation of the inverse of a hypergeometric function is computationally expensive [39, 40]. Thus, we computed CDF, $F(v)$ numerically at higher resolution by choosing minimal values of velocity intervals $\Delta v = 0.5/N_p$. This numerically estimated CDF is then used to assign velocity to Np number of particles using the inverse CDF method. It may be noted that we have total Np number of particles in the simulation system such that $\int_{-\infty}^{+\infty} f(v)dv = Np$. Analytically the velocity space can have limits of $-\infty$ to $+\infty$, but in the simulation system, the maximum limit of the velocity is taken as $v_{max} = 10v_{th}$, so that all Np number of particles are located within $[-v_{max}, +v_{max}]$. First, we obtained the velocities of $Np/2$ ($=F(v_{max})$) number of particles in $[0, v_{max}]$ space and then assigned same magnitude of velocity to remaining $Np/2$ particles in $[-v_{max}, 0]$ velocity space.

Furthermore, we used the same method to generate particles that follow the thermal distribution function. This distribution has the following form of the CDF,

$$F(v) = \int_0^v f(v)dv = \frac{n_0}{\sqrt{2\pi}v_{th}} erf\left[\frac{v^2}{\sqrt{2}v_{th}}\right] \tag{3}$$

Both kappa and Maxwellian distribution functions are developed in MATLAB. The MATLAB functions to generate particles that follow kappa and Maxwellian distributions in velocity space are given in appendices A and B.

In order to verify the performance of these functions, we generated particles following kappa distribution using (i) inverse CDF method (used in the present study), and (ii) the student t-distribution (proposed by Abdul *et al* [32]) and compared them with its theoretical form as shown in figure 1(a). We consider the thermal velocity of the particle $v_{th} = 1$, a number of particles $Np = 5 \times 10^5$, and kappa index $\kappa = 2$ to ensure significant nonthermality. The difference between the theoretical and simulated kappa distribution function using

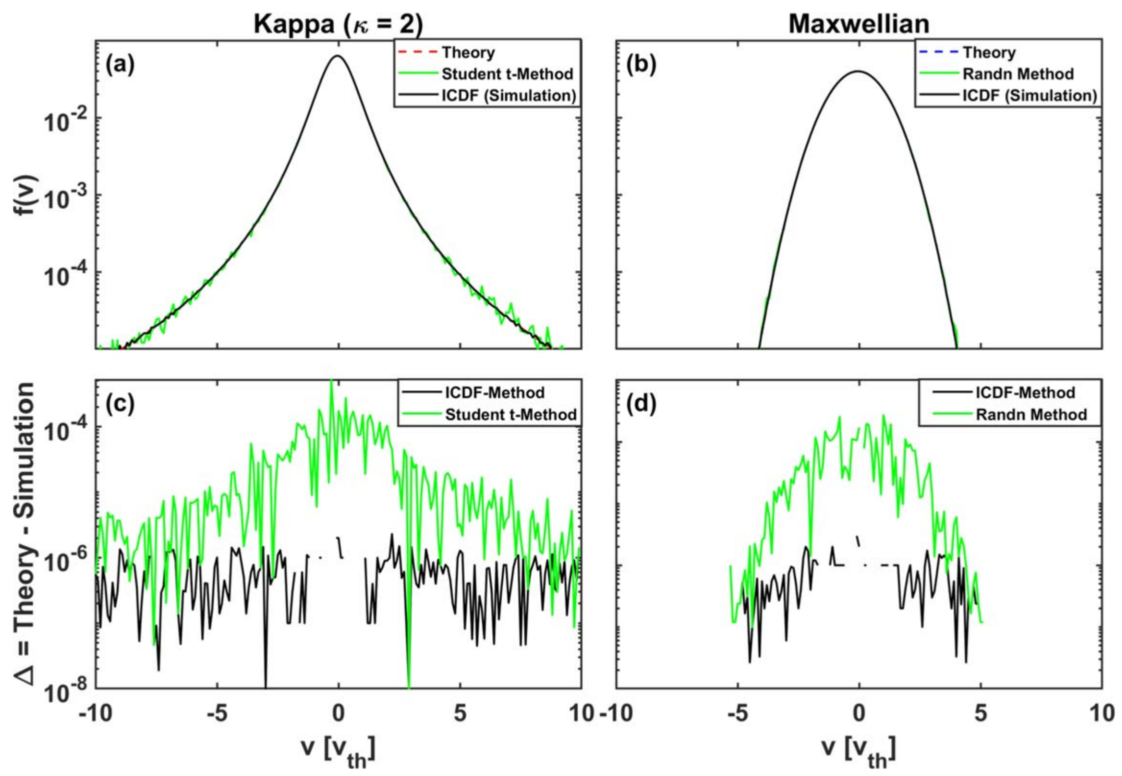

Figure 1. (a) The kappa distribution function generated using inverse CDF method (black color), the student t-distribution function (green color) and its theoretical form (red dotted line). (b) The Maxwellian distribution function generated using the inverse CDF method (black colour) and from random number method (green colour) is compared with its theoretical form (blue dotted line). The difference between the theoretical and simulated kappa and Maxwellian distribution functions are plotted in panels (c) and (d), respectively.

respective methods are plotted in figure 1(c). The kappa distribution generated using the inverse CDF method (black color) produces less error in the tail of the distribution function than the method based on the student t-distribution. Similarly, in figure 1(b), the Maxwellian distribution function generated using the inverse CDF method and random number method is compared with its theoretical form. The difference between the theoretical and simulated Maxwellian distribution function using respective methods are plotted in figure 1(d). Figure 1 indicate that both Maxwellian and kappa distribution functions generated using the inverse CDF method are in good agreement with their respective theoretical forms In the following subsection, we describe the governing equations and initial conditions of the simulation system to understand the effects of particle distribution function on wave-particle interaction dynamics.

2.2. Governing equations and initial conditions of simulation system

We study dynamics of electrons following thermal or nonthermal distribution function, moving along a stationary electrostatic positive wave potential using a test-particle simulation approach. The simulation system consider only electrons as positive wave potential will not effect the ion dynamics. For simplicity, we assume a one-dimensional system of length $L\left(x = -\frac{L}{2} \text{ to } +\frac{L}{2}\right)$ with a periodic boundary condition in the absence of background magnetic field (i.e. $B_0 = 0$). The equation of motion of the particle with charge q and mass m in the presence of wave electric field $\mathbf{E_w}$ can be written as,,

$$\frac{d\mathbf{v}}{dt} = \frac{q}{m}\mathbf{E_w}, \tag{4}$$

$$\frac{d\mathbf{x}}{dt} = \mathbf{v}. \tag{5}$$

We observe the wide variety of electric field structures in space plasmas. Among these, coherent solitary waves are observed everywhere in the Earth's magnetosphere. These waves mostly propagate parallel to the magnetic field and are treated as electrostatic solitary waves (ESWs). These wave structures are observed as unipolar, bipolar, or even tripolar pulses in high-resolution electric field measured by spacecraft [41–43]. However, the ubiquitous observation of bipolar type structures makes it a potential candidate for study their role in particle trapping [44–46]. The electrostatic potential associated with these bipolar pulses can be model through Gaussian distribution [43]. Therefore, it is reasonable to assume a Gaussian wave potential to model the particle trapping.

The expression of static Gaussian wave potential, ϕ at the center of the simulation system can be written as,

$$\phi(x) = \psi \exp(-x^2/2\delta^2) \tag{6}$$

Here, ψ and δ are the amplitude and width of wave potential. The resultant electric field associated with the wave is given by,

$$E_w(x) = -\frac{d\phi}{dx} = \frac{x\psi e^{-\frac{x^2}{2\delta^2}}}{\delta^2} \tag{7}$$

We assume electrostatic wave with a cold plasma dispersion relation $\omega = \omega_{pe}$, where ω_{pe} is electron plasma frequency. In the simulation , system length (L) is normalized with Debye length (λ_{de}), simulation time is normalized with ω_{pe}^{-1}. The ambient plasma parameter are considered as: plasma density $n_0 = 1$, system length $L = 32\lambda_{de}$, charge to mass ratio $q/m = -1$, kappa index $\kappa = 2$, plasma frequency $\omega_{pe} = 1$, and Debye length $\lambda_{de} = 1$. The equation of motion (4, and 5) are solved numerically by forth-order Runge-Kutta method for 5×10^5 electrons in the presence of wave potential characterized by amplitude ψ and width δ. Here, ψ, δ and time are expressed in the units of mv_{th}^2/e, λ_{de} and ω_{pe}^{-1}, respectively. The equation of motions are solved for velocity v, and position x with $dv = 0.1$, and $dx = 0.1$, in normalized units. The total simulation time is taken as $120\ \ \omega_{pe}^{-1}$ with a time step Δt of $0.2\omega_{pe}^{-1}$, i.e. total 600 steps for all the particles. The results obtained from the simulation are discussed in section 3.

3. Results and discussion

We have examined the role of characteristics of wave potential with the positive polarity and ambient electron velocity distribution function on the process of electron trapping (The similar analogy is applicable for the potential of negative polarity if the species of simulation system is ions). We took different simulation runs by changing the amplitude ($\psi = 1, 2, 4, 6, 8$) and width ($\delta = 1, 2, 4, 6, 8$) of the wave potential. As it is a test particle simulation, the electrons can interact with a wave potential in a self-consistent manner without effecting the ambient parameters. The time evolution of nonlinear trapping of the electron in a stationary Gaussian wave potential is examined. In order to distinguishes trapped electrons from free ones, we have used the well established principle of separatrix [47]. Tobita *et al* [48] performed test particle simulations of electrons in an electrostatic model with Langmuir waves and a non-oscillatory electric field and deduce the trapping region by trapping velocity (v_{trap}), and full width at the half maximum of the wave potential distribution (λ) defined by,

$$v_{trap} = 2\frac{\omega_{tr}}{k} = 2\sqrt{\frac{e}{m}\frac{E_{w0}}{k}} \tag{8}$$

Here, $\omega_{tr} = \sqrt{ekE_{w0}/m}$ is trapping frequency, E_{w0} is peak electric field, $k = 2\pi/\lambda$ is wave vector, The width of wave potential δ is given by $\lambda/2.35$. The electrons whose thermal energy is less than the energy of wave potential will remain trapped electrons inside the potential, and rotate around $\phi(x)$ with ω_{tr} frequency. The other electrons pass outside the potential. The trapping period of trapped particles can be written as, $\tau = \frac{2\pi}{\omega_{tr}} = \sqrt{\frac{2\pi m\lambda}{eE_{w0}}}$. The trapped number of electrons N_{trap} are estimated by integrating electron distribution function $f(x, v)$ in phase space from $-v_{trap}$ to v_{trap} in velocity space, and from $-\frac{\lambda}{2}$ to $+\frac{\lambda}{2}$ in position space. [49, 50].

As an example, the time evolution of nonlinear trapping of electrons (5×10^5) is shown in figure 2 for $\kappa = 2, v_{th} = 1, \psi = 2, \delta = 2$. The first column of figure 2 shows the electrons distribution in phase space at time 0, 10 and 50 ω_{pe}^{-1}. The horizontal and vertical lines in the panels (a), (d) and (g) of figure 2 are corresponding to the trapping region in velocity $(-v_{trap}, v_{trap})$ and position $\left(-\frac{\lambda}{2}, \frac{\lambda}{2}\right)$ space. Similarly, second and third columns of figure 2 respectively shows the distribution function $f(v)$ as a function of v and number density $n(x)$ (in the unit of n_0) as a function of $(x–x_c)$ for corresponding times. Here, x_c represents the center of the simulation system. Orange plot in the middle panels show the change in distribution function concerning the initial distribution function. Since wave potential of specific width and amplitude is present at the center of the simulation system, the electrons of suitable velocity (between $-v_{trap}$ to v_{trap}) and suitable position (between $-\frac{\lambda}{2}$ to $\frac{\lambda}{2}$) get trapped in the wave potential. This results in enhancing the electron density at the center of the simulation system. The leftmost panels of figure 2 show the phase space evolution of the electrons in the presence of the wave potential. At $t = 0$, when we introduce a coherent electrostatic wave into the simulation system, nonlinear interaction of the electrons with wave initiates, and a part of the total electron gets trapped in the wave potential. The presence of a filled circular structure in figure 2 resembles the accumulation of the electrons, and it is the manifestation of electron trapping inside the wave potential.

To examine the effect of amplitude and width of wave potential on electron trapping, first we choose fixed $\delta = 2$ and varied $\psi = 1, 2, 4, 6$ and 8, and secondly, we fixed $\psi = 2$ and varied $\delta = 1, 2, 4, 6$ and 8. These simulation runs were performed separately for kappa and Maxwellian distributions. In this way, we performed a

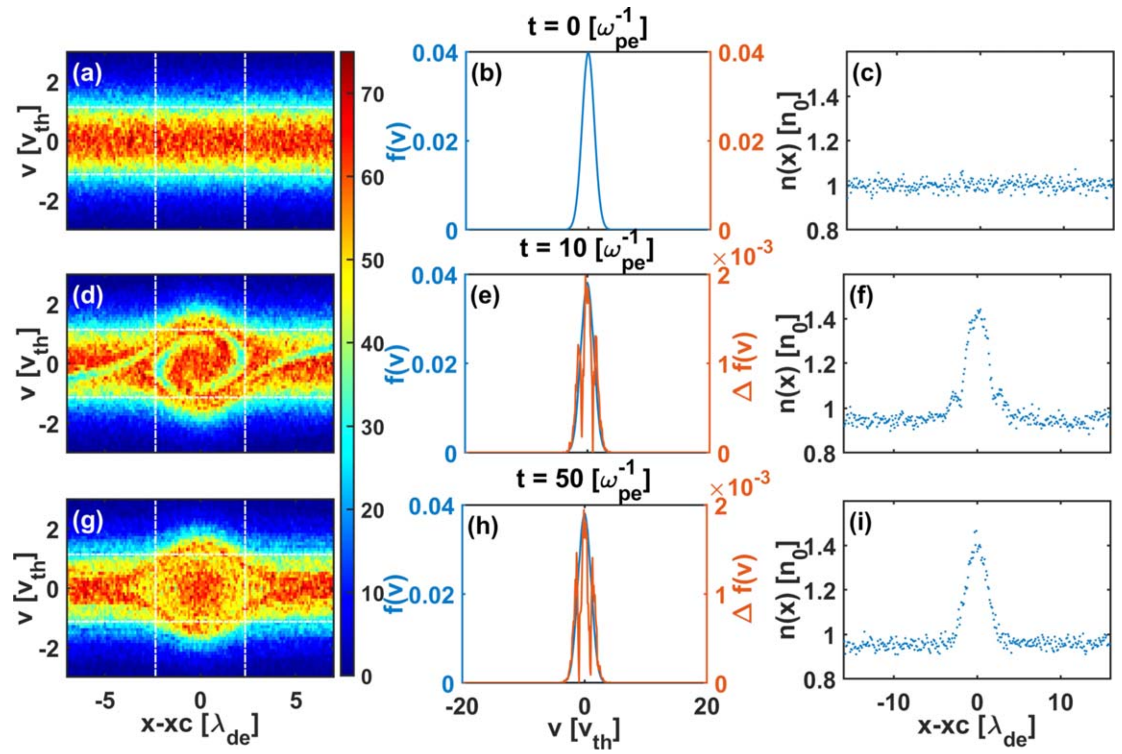

Figure 2. The nonlinear trapping of electrons in the wave potential is shown for the parameters $\kappa = 2, v_{th} = 1, \psi = 2, \delta = 2$. In the first row, panels (a), (b), and (c) respectively shows the distribution of electron in the phase space, electron distribution function $f(v)$ as a function of v, and electron number density n as a function of x at initial time $t = 0$. The change in distribution function with respect to initial distribution function (i.e. $\Delta f(v) = f(v)–f(v, t_0)$) is shown by red dotted lines in the middle panels e and h. In the same manner, the variations of these parameters at time $t = 10$, and $t = 50\omega_{pe}^{-1}$ are depicted in the middle (d), (e), (f) and bottom (g), (h), (i) rows, respectively.

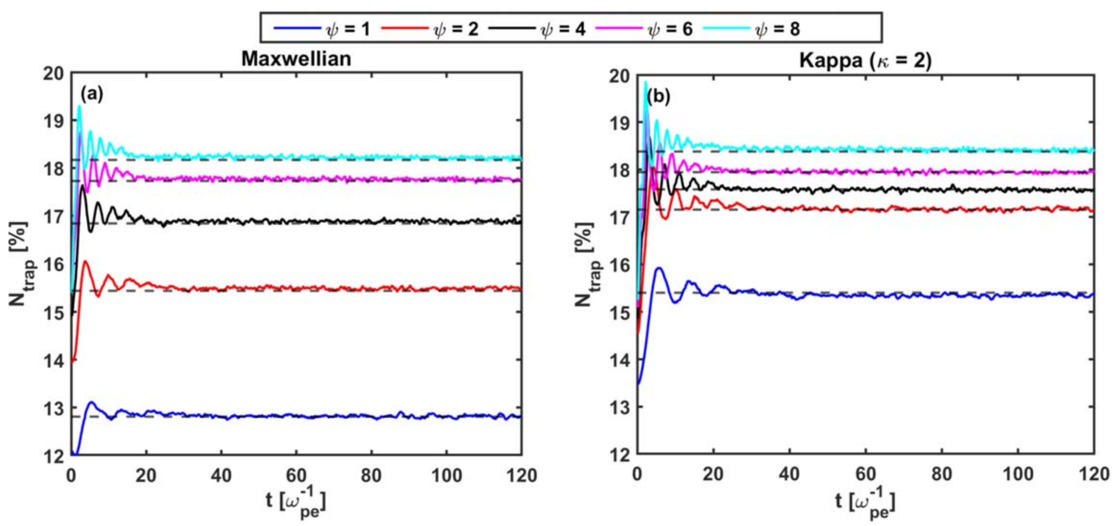

Figure 3. The total number of trapped electrons (N_{trap}) is plotted as a function of time for a fixed value of $\delta = 2$ and by varying ψ as 1, 2, 4, 6, 8 of wave potential. Panels (a) and (b), respectively corresponds to Maxwellian and kappa velocity distribution for ambient electrons. Horizontal black dotted lines indicate the stable electron trapping region.

total of 20 simulation runs. The total number of trapped electrons (N_{trap}) in the wave potential estimated as a function of time for each run is shown in figures 3 and 4. The left and right panels in figures 3 and 4 correspond to Maxwellian and kappa distributions, respectively. When the simulation starts ($t = 0$), all the electrons with non-zero energy will start interacting with the potential, which causes an escalation in the trapped electron population. When an electron gets trapped inside the potential, it oscillates, and it is trapped until it has enough energy to escape the potential barrier. However, as time evolves, electrons with higher energy get out of the

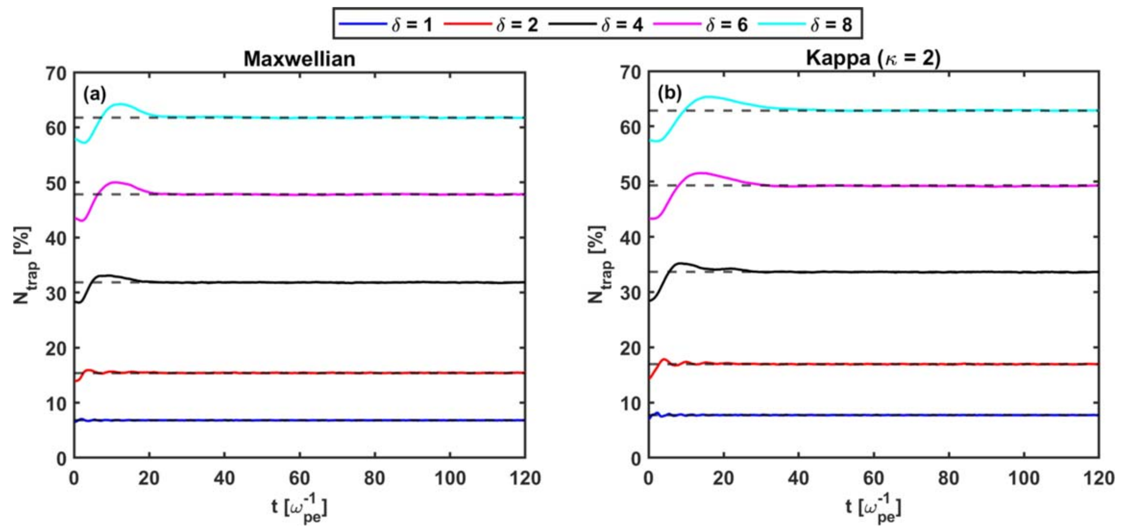

Figure 4. The total number of trapped electrons (N_{trap}) is plotted as a function of time for a fixed value of $\psi = 2$ and by varying δ as 1, 2, 4, 6, 8 of wave potential. Panels (a) and (b), respectively corresponds to Maxwellian and kappa velocity distribution for ambient electrons. Horizontal black dotted lines indicate the stable electron trapping density.

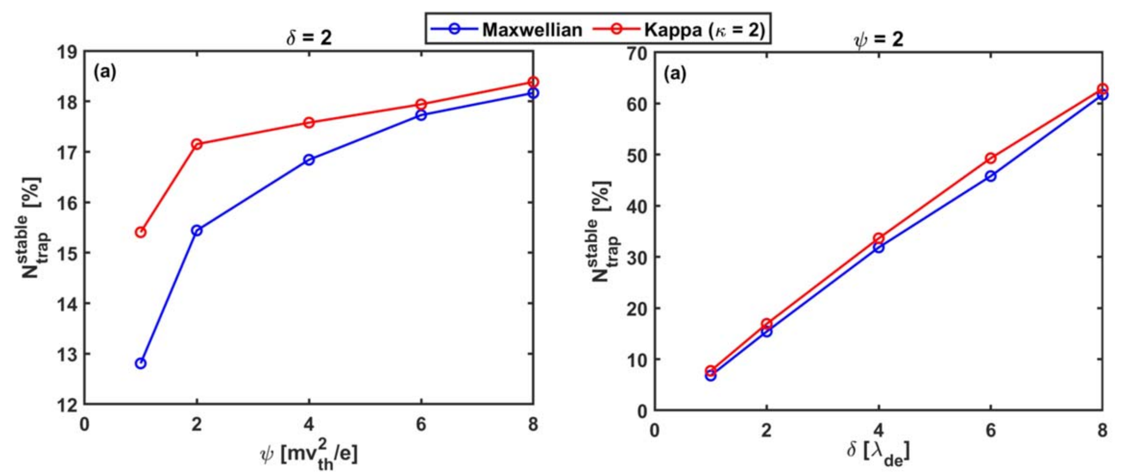

Figure 5. The total number of trapped electrons in the stable region is plotted as a function of (a) amplitude of wave potential ψ for fixed-width ($\delta = 2$) and (b) width of wave-potential δ for fixed amplitude ($\psi = 2$). The blue and red colours represent the case of kappa and Maxwellian electron distribution, respectively.

potential and can be considered untrapped. Others with suitable velocity will be confined in the trapping zone resulting in the stabilization of phase space structure. Therefore, the trapped electron density increases and attains the peak in the staring and then stabilizes by maintaining the nearly constant trapped electron density in each simulation run. The trapped density after stabilization is denoted by N_{trap}^{stable}.

The trapped electron density after stabilization (N_{trap}^{stable}) for each run is plotted as a function of ψ for fixed $\delta = 2$ in figure 5(a), and as a function of δ for fixed $\psi = 2$ in figure 5(b) for kappa (red curve) and Maxwellian (blue curve) electron distribution. It is evident in figure 5 that as amplitude and width of the wave potential increases, the trapped electron population increases. As we increase the amplitude of the potential by keeping the width constant ($\delta = 2$), the electric field energy associated with the wave potential increases, [51]. Analytically, as wave amplitude (ψ) increases, v_{trap} increases, which increases the trapping region in velocity space. Therefore, the wave potential becomes capable of trapping the higher energetic electron, and the number of trapped electrons increases for both Maxwellian and kappa distribution. Similarly, as we increase the width of the potential by keeping the amplitude constant ($\psi = 2$), the electric field energy associated with the wave potential decreases [51]. Therefore, the capacity to trap higher energy electrons reduces. However, in this case, more lower-energy electrons will get trapped. Simultaneously, a wider potential has enough space to accumulate these electrons (as λ increases) and carry out oscillations. Hence the number of trapped electrons increases as the

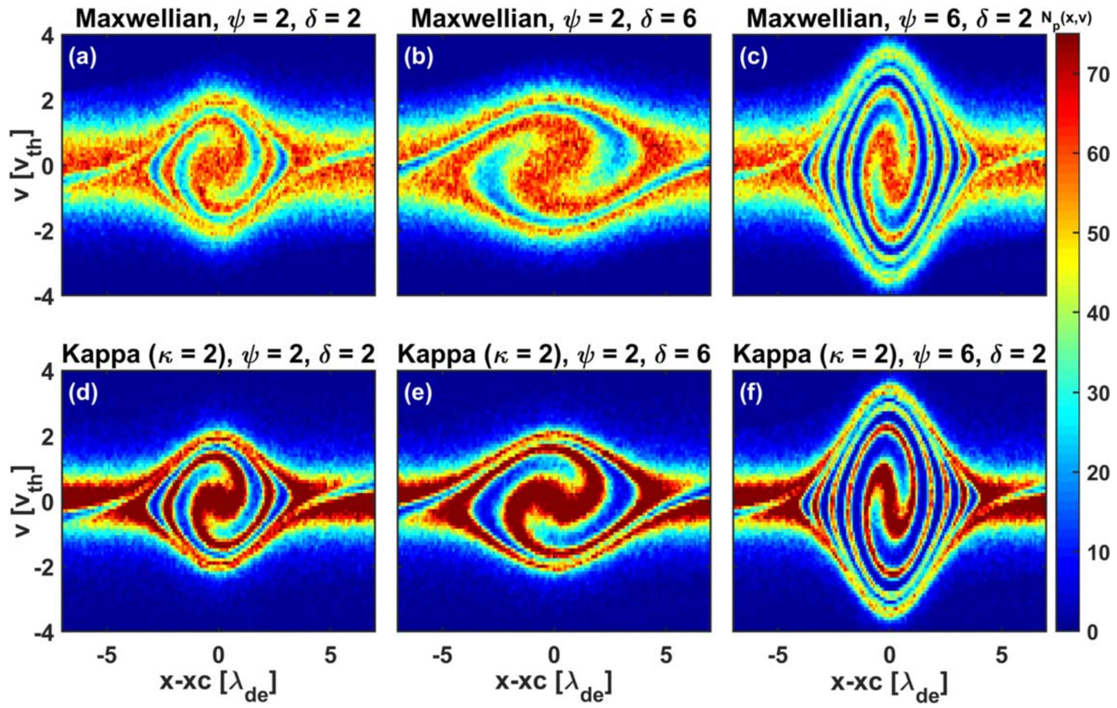

Figure 6. This figure shows the trapped electron population in the phase space for different values of amplitude and width of the wave-potential. The top panels depict the case of Maxwellian electrons, and the bottom panels depict the case of kappa electrons.

width of potential increases. In both scenarios, as we increase the width or amplitude of wave potential, the trapped electron density increases.

Another prominent feature in figure 5 is that for the fixed potential's width ($\delta = 2$), as the amplitude of wave increases, the maximum ~19% electrons traps. On the other hand for fixes amplitude $\psi = 2$, as width increases, maximum ~60% electrons traps. It is because, as the width of wave potential increases, the potential traps more electrons having lower energy. Also, increased width results in the increased spatial extent (λ). Both these effects simultaneously increase the number of trapped electrons for the increased width. Hence we can conclude that a coherent wave-potential with larger width traps a larger number of electrons than the one with a larger wave amplitude.

Moreover, it is evident from figures 3, 4, and 5 that, irrespective of varying amplitude or width of wave potential, the trapped electron density is more for electrons following kappa distribution than Maxwellian distribution. It indicates that trapping is more efficient in nonthermal plasma, and it demands a larger trapped population to attain stability. The reason for this is the less thermal velocity of the electrons in kappa distribution ($v_{th} = \sqrt{(2\kappa - 3)k_B T/m\kappa}$) as compare to that of Maxwellian ($v_{th} = \sqrt{k_B T/m}$). As the kappa distribution function is steeper than the Maxwellian; it possesses lower thermal velocity for a maximum number of particles than that of Maxwellian [28]. In electron trapping, particles with lower energy are likely to get trapped easily, whereas those with higher energy can escape from the potential. For kappa distributed electrons, having lower thermal energy are more. Hence, they largely get trapped as compared to the case of electrons following Maxwellian distribution.

The phase-space plot of electrons for different combination of ψ and δ are depicted in figure 6 at time $t = 10\omega_{pi}^{-1}$ as vortex-type structures. The upper panels (a)–(c) are for the ambient electrons following Maxwellian distribution, and the lower panels (d)–(f) are for the kappa distribution. Physically, the trapped particles inside the potential oscillate, and these oscillations are evinced as vortex-type structures. Analytically, one can derive the generalized expression for the position and velocity of the electron trapped in a wave field (like $E = E_{w0}e^{-ikx}$). The position and velocity are respectively given by $x = eE_{w0}\,cos(kx)/mw_{trap}^2$ and $v = eE_{w0}sin(kx)/mw_{trap}$. It may be noted that the position and velocity have cosine and sine terms, respectively. Thus in phase space, this oscillatory motion appears as the vortex-type structures. Figure 6 demonstrates the variation of electron trapping with the amplitude and width of the wave potential for Maxwellian and kappa distributed electrons. The color bar represents the number of electrons distributed in phase space, and evident that for the same wave amplitude and width, the trapping is more for the kappa distribution as compared to the Maxwellian distribution. Hence we can conclude that the wave potential traps more electrons when electrons follow kappa distribution.

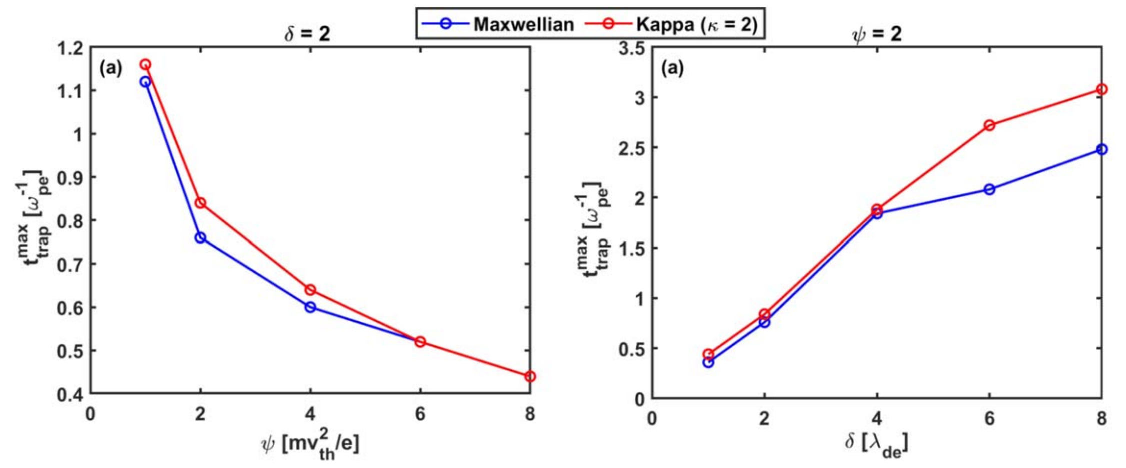

Figure 7. The time of maximum trapping t_{trap}^{max} in the wave potential is plotted as a function of (a) amplitude, ψ and (b) width δ of wave potential for both Maxwellian and kappa electrons.

Next, we have investigated the effects of wave potential and width on the time of maximum trapping. Figures 3, and 4 indicate the behavior of trapped electrons for wave potentials of different amplitude and width, respectively. The curve's peak represents the maximum trapped electron density, and corresponding time is referred to as the time of maximum trapping, t_{trap}^{max}. To understand the trapping time dependence on potential amplitude and width, we noted the time of maximum electron trapping (t_{trap}^{max}) and plotted it as a function of the amplitude and width of wave potential in figures 7(a) and (b), respectively for Maxwellian (blue) and kappa (red) distributions. Figure 7(a) evident that as the amplitude of wave-potential increases, the time required to reach a stable trapping state decreases, i.e. a higher amplitude potential can reverberate with stability faster. It is because, for a higher amplitude potential, higher energy particles will get trapped inside it, and as a result, fast oscillations happen inside the potential (i.e. trapping time τ decreases). Thus the effective screening will happen quickly, and the structure will stabilize quickly. Thus, we can say that for stronger wave potential, a stable trapping state occurs faster. Similarly, in figure 7(b) evident that as the width of the potential increases, the time required to reach a stable trapping state also increases, i.e. a wider potential requires a higher time to stabilize. The higher energetic particles only get trapped if the amplitude increases, it has no relation with the width of the potential. Therefore, as the width of potential increases, slow oscillations happen inside the potential (i.e. trapping time τ increases); as a result, the particles need to oscillate for a longer time to screen out the potential. Thus, for wider wave potential, a stable trapping state occurs slower. Conclusively we can say that the coherent wave with a larger amplitude traps electrons faster than the wave potential with lower amplitudes.

4. Summary and conclusions

We have investigated the nonlinear trapping of electrons in the presence of an electrostatic wave and its dependence on the characteristics of the wave potential and the ambient velocity distribution function of plasma. The simulation model consists of a stationary positive coherent wave potential and a large number of electrons (5×10^5) following Maxwellian or kappa distribution.

A new approach is presented to distribute the electrons following kappa distribution in velocity space using the inverse CDF method. The inverse CDF method is compared with the existing student t-distribution method [32] and found to have very less deviation from analytical expression, particularly in the tail side where higher energetic particles are situated. The MATLAB code is provided (appendices A and B) to distribute the particle following kappa and Maxwellian distribution, which can be used in particle simulations for general purposes. Electrons following Maxwellian or kappa distribution are initiated in the simulation model in the presence of positive wave potential of different amplitudes and widths. A similar analogy is applicable for negative wave potential if the species is an ion. The simulation demonstrates that the width and amplitude of coherent wave-potential constructively control the trapped electron density. It is noted that trapped electron density varies from 10%–60% when the width of wave potential varied from 1–8 [λ_{de}] and varies from 13%–19% when the amplitude of wave potential varied from 1–8 [mv_{th}^2/e]. Besides, the ambient electron velocity distribution plays a vital role in determining the trapped electron population. It is noted that for a given potential structure, the electron trapping is more plasmas having kappa distribution as compare to Maxwellian distribution. The average thermal velocity of electrons is less for electrons following kappa distribution as compared to

Maxwellian, therefore they gets trap easily leading to higher trapped densities of electrons in nonthermal plasmas. In addition, the simulation shades light on the variation of time of maximum trapping (t_{trap}^{max}), with amplitude and width of wave potential and concludes that the coherent wave with a larger amplitude traps electrons faster as compare to the wave potential with lower amplitudes.

In space and laboratory plasma, since the wave potential's width and amplitude vary depending on their generation process, the associated electron trapping phenomena also likely to vary. The role of wave characteristics in particle trapping is evident in our study. It implies that the processes like plasma transport and plasma heating will be affected considerably in the presence of coherent wave structures. Secondly, as the recent studies reveal that kappa distribution describes the energy equilibrium in space plasmas, this kind of study, which addresses the difference in the particle trapping for thermal and nonthermal plasmas, will be of great interest. Also, the new approach to generate particles following kappa distribution presented in the paper will be useful for general space plasma simulation modeling. The primary outcomes of the study are summarized below.

- An efficient method for generating the particles in the form of kappa distribution is developed using the inverse CDF method in MATLAB.
- A one-dimensional test particle simulation is performed to examine the effect of velocity distribution function on an electron's trapping in a stationary coherent wave-potential of positive polarity.
- The number of trapped electrons inside the static wave potential increases with amplitude and width due to increased trapping zone in the phase space.
- A coherent wave-potential with larger potential width (spatial extents) traps a larger number of electrons than the one with larger wave amplitude.
- The coherent wave with a larger amplitude traps electrons faster as compare to the wave potential with lower amplitudes. This tendency can be understood from trapping period, which is given by the $\tau = \sqrt{\frac{2\pi m\lambda}{eE_{w0}}}$. It implies that the electron oscillates slowly if the wave potential has a larger width and a smaller amplitude.
- The particle trapping is found to be more efficient in nonthermal plasmas than thermal plasma. This tendency is in agreement with the theoretical study carried out by Aravindakshan *et al* [29] and it is attributed to the lower average thermal velocity of kappa distributed particles. In general, this tendency can assist in transporting more plasma particles from one region to another through waves more effectively in nonthermal plasmas as compared to thermal plasmas.

The present study will be helpful to understand the particle trapping by the coherent waves, which are frequently seen in space and astrophysical plasmas.

Acknowledgments

The model computations were performed on the High-Performance Computing System at the Indian Institute of Geomagnetism.

Data availability statement

The data that support the findings of this study are available upon reasonable request from the authors.

Appendix A. Generating particles following kappa distribution function

The following MATLAB function generates 'n' particles in velocity space following kappa distribution with desired thermal velocity (v_{th}), drift velocity (v_d), and kappa index (κ). For this we have generated a total of N_p ($=2^{24}$) particles using inverse CDF methods, and than choosing 'n' particles of them using bit reversal operator to achieve less numerical deviation from analytical expression.

```
%   kappafunction.m—Generate particles in velocity space that follows kappa
%   distribution. To perform this inverse cummulative distribution function is used.
%   In this method, total 2^24 are generated, and then 'n' particles are chosen to achieve numerical accuracy.
function vv = kappafunction(kp, n, vth, vd)
%   Inputs
```

(Continued.)

```
%        kp   :   kappa index (greater than 1.5)
%        n    :   Number of particles (greater than 10^5 for reasonable accuracy and less than 2^24 to avoid system limits)
%        vth  :   Thermal velocity of particle
%        vd   :   Drift Velocity
%
%   Outputs
%        vv   : are velocity of 'n' number of particles
%%
%   Intial calculations
Np      =   2^24;
dvchk   =   0.5/Np;
vchk    =   0: dvchk: 10*vth;
Nph     =   Np*0.5;
fvchk   =   zeros(1, length(vchk));

%   Generating the cumulative kappa distribution function (CDF) numerically
g     =   gamma(kp + 1)/gamma(kp-0.5); %   Constant
con   =   g/(kp*sqrt(pi*(2*kp-3)));     %   Constant
con1  =   2*kp-3;                       %   Constant

%   Compute alpha, so that number of particles under fv for [0 vmax] is Nph
alpha     =   Nph/(con*10*hypergeom([0.5, kp],1.5, -10.^2/con1));
sum       =   0;
for i     =   1: length(vchk)
fv        =   (1+(vchk(i)*vchk(i)/con1)).^-kp;
fvchk(i)  =   sum;
sum       =   sum + fv;
end
fvchk=fvchk*alpha*con*dvchk;

%   Use of inverse CDF for assigning velocities to the particles
v  =  zeros(1, Nph); m  =  1;
for j  =  1: Nph
    chk  =  0;
    while m  <  length(fvchk)  &&  chk  ==  0
        if fvchk(m)>j
            chk  =  1;
        else
            v(j)  =  0.5*(vchk(m) + vchk(m + 1));
            m  =  m + 1;
        end
    end
end
clear   fvchk;   clear   vchk
v  =  [0-flip(v) v];
v  =  v.*vth + vd;
i  =  bitrevorder(1: Np);
v  =  v(i);   vv  =  v(1: n);         % Choosing 'n' particles from Np
end
```

Appendix B. Generating particles following maxwellian distribution function

The following MATLAB function generates 'n' particles in velocity space following Maxwellian distribution with desired thermal velocity (v_{th}), and drift velocity (v_d). We are using the same method here as wi used to generate particle following kappa distribution.

```
%   maxwfunction.m- Generate particles in velocity space that follows
%   maxwellian distribution. To perform this inverse cummulative distribution function is used.
%   In this method, total 2^24 are generated, and then 'n' particles are chosen to achieve numerical accuracy.
function vv  =  maxwfunction(n, vth, vd)
%   Inputs
```

(Continued.)

```
%      n      :   Number of particles (greater than 10^5 for reasonable accuracy and less than 2^24 to avoid system limits)
%      vth    :   Thermal velocity of particle
%      vd     :   Drift Velocity
%
%   Outputs
%      vv     :   are velocity of 'n' number of particles
%%
%   Intial calculations
Np      =   2^24;
Nph     =   Np*0.5;
con     =   sqrt(pi/2);
v       =   zeros(1, Nph);
vmax    =   10*vth;

%   Compute alpha, so that number of particles under fv for [0 vmax] is Nph
alpha      =   Nph/(con*erf(vmax/sqrt(2)));

%   Use of inverse CDF for assigning velocities to the particles
for   j  =  1:Nph
v(j)  =  sqrt(2)*erfinv((j/(alpha*con)));
end

v  =  [0-flip(v) v];
v  =  v*vth + vd;
i  =  bitrevorder(1:Np);
v  =  v(i); vv  =  v(1:n);          %  Choosing 'n' particles from Np
end
```

ORCID iDs

Pankaj K Soni https://orcid.org/0000-0002-0930-3900
Harikrishnan Aravindakshan https://orcid.org/0000-0003-4663-4255

References

[1] Tejero E, Crabtree C, Blackwell D, Amatucci W, Mithaiwala M, Ganguli G and Rudakov L 2015 *Sci. Rep.* **5** 17852
[2] Zestanakis P, Kominis Y, Hizanidis K and Ram A 2013 *Phys. Plasmas* **20** 072507
[3] Wilson L III, Cattell C A, Kellogg P J, Wygant J R, Goetz K, Breneman A and Kersten K 09/09/2011 *Geophys. Res. Lett.* **38** 17
[4] Tochitsky S Y, Narang R, Filip C, Musumeci P, Clayton C, Yoder R, Marsh K, Rosenzweig J, Pellegrini C and Joshi C 2004 *Phys. Plasmas* **11** 2875–81
[5] Thorne R M, Bortnik J, Li W and Ma Q 2021 *Magnetospheres in the Solar System* (USA: American Geophysical Union (AGU)) 93–108
[6] Khazanov G V and Chen M W `14/05/2021 *Journal of Geophysical Research: Space Physics* **126** e2021JA029211
[7] Allison H J, Shprits Y Y, Zhelavskaya I S, Wang D and Smirnov A G 2021 *Science Advances* **7** eabc0380
[8] Matsumoto H, Kojima H, Miyatake T, Omura Y, Okada M, Nagano I and Tsutsui M 1994 *Geophys. Res. Lett.* **21** 2915–8
[9] Wang R *et al* 2020 *Astrophys. J. Lett.* **889** L9
[10] Baumjohann W and Treumann R A 1997 *Basic Space Plasma Physics* (Singapore: World Scientific)
[11] Chen F F *et al* 1984 *Introduction to Plasma Physics and Controlled Fusion* vol 1 (Berlin: Springer)
[12] Artemyev A, Neishtadt A, Vainchtein D, Vasiliev A, Vasko I and Zelenyi L 2018 *Commun. Nonlinear Sci. Numer. Simul.* **65** 111–60
[13] Tsurutani B T and Lakhina G S 1997 *Rev. Geophys.* **35** 491–501
[14] Luque A and Schamel H 2005 *Phys. Rep.* **415** 261–359
[15] Aravindakshan H, Kakad A and Kakad B 2018 *Phys. Plasmas* **25** 122901
[16] Vasko I, Krasnoselskikh V, Mozer F and Artemyev A 2018 *Phys. Plasmas* **25** 072903
[17] Bernstein I B, Greene J M and Kruskal M D 1957 *Phys. Rev.* **108** 546–50
[18] Krasovsky V L, Matsumoto H and Omura Y 2006 *Phys. Scr.* **74** 227–31
[19] Artemyev A, Neishtadt A, Vasiliev A and Mourenas D 2017 *Phys. Rev.* E **95** 023204
[20] Yoon P H, Rhee T and Ryu C M 2005 *Phys. Rev. Lett.* **95** 215003
[21] Saini N, Kourakis I and Hellberg M 2009 *Phys. Plasmas* **16** 062903
[22] Pierrard V and Lazar M 2010 *Sol. Phys.* **267** 153–74
[23] Maharaj S and Bharuthram R 2017 *Phys. Plasmas* **24** 022305
[24] Elkamash I and Kourakis I 2021 *Sci. Rep.* **11** 1–11
[25] Elkamash I S and El-Hanbaly A M 2021 *J. Phys. A: Math. Theor.* **54** 065701
[26] Lotekar A, Kakad A and Kakad B 2019 *Commun. Nonlinear Sci. Numer. Simul.* **68** 125–38
[27] Singh K, Kakad A, Kakad B and Saini N S 2021 *Mon. Not. R. Astron. Soc.* **500** 1612–20

[28] Livadiotis G 2017 *Kappa Distributions: Theory and Applications in Plasmas* (Amsterdam: Elsevier)
[29] Aravindakshan H, Kakad A and Kakad B 2018 *Phys. Plasmas* **25** 052901
[30] Robert C and Casella G 2013 *Monte Carlo Statistical Methods* (Berlin: Springer)
[31] Martino L 2018 *Independent Random Sampling Methods* (Berlin: Springer)
[32] Abdul R and Mace R 2014 *Comput. Phys. Commun.* **185** 2383–6
[33] Gao Z, Zhu H, Zhang L, Zhou Q, Yang C and Xiao F 2014 *Astrophys. Space Sci.* **351** 427–34
[34] da Silva C L, Denton R E, Hudson M K, Millan R M, Liu K and Bortnik J 2018 *Geophys. Res. Lett.* **45** 5234–45
[35] Schippers P *et al* 2008 *Journal of Geophysical Research: Space Physics* **113**
[36] Carbary J, Kane M, Mauk B and Krimigis S 2014 *Journal of Geophysical Research: Space Physics* **119** 8426–47
[37] Omura Y 2007 *Advanced Methods for Space Simulations* ed H Usui and Y Omura (Tokyo: Terra Sci.) pp 1–21
[38] Hikishima M, Yagitani S, Omura Y and Nagano I 2009 *Journal of Geophysical Research: Space Physics* **114**
[39] Pearson J W 2009 Computation of hypergeometric functions *Ph.D. Thesis* University of Oxford
[40] Pearson J W, Olver S and Porter M A 2017 *Numer. Algorithms* **74** 821–66
[41] Jovanovic D, Shukla P and Morfill G 2005 *J. Plasma Phys.* **71** 203
[42] Lakhina G, Singh S, Kakad A, Goldstein M, Vinas A and Pickett J 2009 *Journal of Geophysical Research: Space Physics* **114**
[43] Kakad A, Kakad B, Anekallu C, Lakhina G, Omura Y and Fazakerley A 2016 *Journal of Geophysical Research: Space Physics* **121** 4452–65
[44] Bale S, Kellogg P, Larsen D, Lin R, Goetz K and Lepping R 1998 *Geophys. Res. Lett.* **25** 2929–32
[45] Cattell C, Dombeck J, Wygant J, Hudson M, Mozer F, Temerin M, Peterson W, Kletzing C, Russell C and Pfaff R 1999 *Geophys. Res. Lett.* **26** 425–8
[46] Pickett J S *et al* 2005 *Nonlinear Processes Geophys.* **12** 181–93
[47] Schamel H 1972 *Plasma Phys.* **14** 905
[48] Tobita M and Omura Y 2018 *Phys. Plasmas* **25** 032105
[49] Matsumoto H and Omura Y 1981 *Journal of Geophysical Research: Space Physics* **86** 779–91
[50] Kakad B, Kakad A and Omura Y 2014 *Journal of Geophysical Research: Space Physics* **119** 5589–99
[51] Griffiths D J 2005 *Introduction to Electrodynamics*